Improved infrared thermography method for fast estimation of complex phase diagrams

Clément Mailhé, Marie Duquesne, Imane Mahroug, Elena Palomo del Barrio

▶ **To cite this version:**

Clément Mailhé, Marie Duquesne, Imane Mahroug, Elena Palomo del Barrio. Improved infrared thermography method for fast estimation of complex phase diagrams. Thermochimica Acta, 2019, 675, pp.84 - 91. ⟨10.1016/j.tca.2019.03.005⟩. ⟨hal-03484783⟩

HAL Id: hal-03484783

https://hal.science/hal-03484783v1

Submitted on 20 Dec 2021

HAL is a multi-disciplinary open access archive for the deposit and dissemination of scientific research documents, whether they are published or not. The documents may come from teaching and research institutions in France or abroad, or from public or private research centers.

L'archive ouverte pluridisciplinaire **HAL**, est destinée au dépôt et à la diffusion de documents scientifiques de niveau recherche, publiés ou non, émanant des établissements d'enseignement et de recherche français ou étrangers, des laboratoires publics ou privés.

Distributed under a Creative Commons CC BY-NC 4.0 - Attribution - Non-commercial use - International License

Version of Record: https://www.sciencedirect.com/science/article/pii/S0040603118307408
Manuscript_f10df97027389cedae99f6fcfbdb6ef4

Improved infrared thermography method for fast estimation of complex phase diagrams

Clément Mailhé[a*], Marie Duquesne[b], Imane Mahroug[b], Elena Palomo del Barrio[c]

[a] *Université de Bordeaux, CNRS, I2M Bordeaux, Esplanade des Arts et Métiers, 33400 Talence, France*

[b] *Bordeaux INP, CNRS, I2M Bordeaux, ENSCBP, 16 avenue Pey Berland, 33600 Pessac, France*

[c] *CIC energiGUNE Parque Tecnológico de Álava, Albert Einstein, 48. Edificio CIC, 01510 Miñano, Álava, Spain*

*Corresponding author: Fax: +33 (0)5.56.84.54.36 Email: clement.mailhe@u-bordeaux.fr

ABSTRACT: Phase diagrams are a primordial tool in materials science, gathering key information for the materials synthesis and the understanding of their formation processes. Numerous experimental techniques exist to determine the phase diagram of a binary system but they are time-consuming. The previously developed IRT method (InfraRed Thermography) enabled the fast determination of preliminary phase diagrams of polyols binary systems in which only liquid-solid and eutectic transitions occur. This method thus allows accelerating their screening step which is crucial before each development of a new material. This work aims at improving the transitions detection and at adapting the IRT method to more complex phase diagrams containing eutectic, peritectic and metatectic transitions. To do so, the phase diagram of the capric-palmitic fatty acids binary system is experimentally determined using the improved IRT method. It is then compared with those obtained using standard Differential Scanning Calorimetry measurements (DSC) and an improved thermodynamic model. Eventually, the limiting factors and the parameters of influence such as the material droplet size, as well as the nature and roughness of the substrate are investigated and discussed.

KEYWORDS: *Phase diagrams, Infrared thermography, detection of transitions, droplet size, roughness of the substrate*

NOMENCLATURE:

Symbols

R	Universal gas constant (J/mol.°C)
Ra	Arithmetical mean roughness (µm)
Rz	Ten-point mean roughness (µm)
T_{amb}	Ambiant temperature (°C)
T_m	Melting temperature (°C)
x_i	Molar fraction
Z_i	Time-eigenfunction

Greek symbols

$\Delta_m h$	Molar melting enthalpy (J/mol)

© 2019 published by Elsevier. This manuscript is made available under the CC BY NC user license
https://creativecommons.org/licenses/by-nc/4.0/

$\Delta_{tr}h$	Molar transition enthalpy (J/mol)
$\Delta_r G^0$	Gibbs free energy of reaction (J/mol)
γ	Activity coefficient
ν	Stoichiometric coefficient

Acronyms

CA	Capric acid
DL	Digital-Level
DSC	Differential Scanning Calorimetry
DTA	Differential Thermal Analysis
FA	Fatty acids
IRT	Infrared thermography
PA	Palmitic acid
SAM.SSA	Sugar Alcohol based Materials for Seasonal Storage Applications

1. Introduction

The need for innovative materials fulfilling precise specifications for given environments has increased exponentially across Europe. Meanwhile, their time-to-market has been shortened. The feasibility of studying a large amount of systems in a short period of time, the understanding and mastering of the manufacturing process to get materials with properties matching a targeted industrial application, represent current scientific and technological challenges with major economic stakes for the industry. In several industrial branches (*i.e.* cosmetic industry, pharmaceutical industry, agri-food industry, metallurgy *etc.*), the research and development of new materials, with improved or new properties, is fundamental and often requires a prior screening step. The time needed for this step would be greatly reduced if a fast and reliable method for phase diagram determination is available.

Two categories of methods are used for estimating phase diagrams [1]: the dynamic methods and the static methods. Contrary to the dynamic methods, the static ones such as microstructure analysis, optic metallography, electron microscopy or X-ray diffraction, allow the study of the behavior of a system at equilibrium or at a local equilibrium state [2]. The dynamic methods consist in continuously monitoring physical properties (thermal, electrical, mechanical) evolving during the cooling and/or heating of a system and in detecting abrupt changes of these properties when a phase change occurs. Amongst these methods, the most commonly used ones are Differential Scanning Calorimetry (DSC) and Differential Thermal Analysis (DTA). DSC presents an advantage over the DTA since it also measures precisely the enthalpy of each occurring phase change in addition to the determination of phase transition temperatures [3-5]. However, the determination of a reliable phase diagram *via* these standard methods is really time-consuming and hence expensive, which does not match with screening procedures. For such purposes, an innovative method based on infrared thermography called IRT-method was thus proposed in [2, 6]. This IRT method was developed in the framework of the European FP7 Research Project SAM.SSA (2012-2015) and validated for the study of simple phase diagrams of polyols (liquid-solid and eutectic transitions). It then allowed for the establishment of preliminary phase diagrams of sugar alcohols binary systems in a few hours only.

Improvements to the IRT method are proposed in this paper with the objective of allowing the estimation of phase diagrams with transitions of increasing complexity (liquid-solid, peritectic, metatectic, *etc.*). Several parameters of influence are identified with regards to the experimental conditions or to the post-treatment. As for parameters influencing the experiment itself, two key

parameters are studied: the sample size and the nature of the substrate material on which are deposited the samples. For each chosen parameter, two experiments are performed in order to assess the influence of each one. One the one hand, as the samples consist of droplets, the influence of their size is studied with regard to their diameter. Hence, two droplet diameters are studied in this work: 3mm and 7mm. On the other, two substrate materials (one made of Aluminum and the other of Brass) are considered in the experiments in order to identify the influence of their natures and of their surface roughness on the obtained results.
Regarding post-treatments, improvements brought to the method and dealing with data-treatment automation and equilibrium modeling are also discussed. The results obtained *via* our improved method are compared and validated with experimental results either obtained by DSC measurements and through thermodynamic modeling or extracted from literature. The conclusions regarding the influence of the studied parameters are finally assessed and perspectives are drawn for the further exploration of the limits of the IRT method.

2. Methodology

2.1 Materials and samples

2.1.1 Materials and tested binary system

The materials used in this work are fatty acids: capric acid (CA) and palmitic acid (PA). Information regarding their origin and their purity as well as key thermophysical properties for this study is reported in Table 1 for comparative purposes. Part of these properties was collected from other works [7-10] while the other was obtained using DSC (see sub-section 2.5.2).

Table 1
General information about the tested materials

Materials	**Capric acid**	**Palmitic acid**
CAS number	334-48-5	57-10-3
Acronym	CA	PA
Supplier	Sigma Aldrich	Sigma Aldrich
Batch Number	BCBJ3927	SLBQ886V
Purity (%)	98	99
Formula	$C_{10}H_{20}O_2$	$C_{16}H_{32}O_2$
Molar mass (g/mol)	172.26	256.43
T_m (°C) in this work (IRT)	33	62.5
T_m (°C) from literature	30.8 [9], 31.3 [8], 31.6 [8], 32.31 [10]	62.4 [9], 61 [8], 63 [8], 64.07 [10]
$\Delta_m h$ (kJ/mol)	27.39 [9], 28.09 [8]	52.31 [9], 52.16 – 54.36 [8]

The binary system studied in this work consists of capric acid (CA) and palmitic acid (PA) because its phase diagram estimation would challenge the initial version of the IRT method. The first use of the IRT method was indeed limited to the detection of liquidus line transitions and eutectic transitions whereas this system appears to include additional transitions such as peritectic and metatectic transitions as suggested in [10].

2.1.2 Sample preparation and experimental set up

The droplets of the CA-PA binary system, each with a specific molar fraction of both components, were deposited on a thin plate (the substrate). In order to have a significant amount of data, the droplets composition ranged from 0 to 100% of CA with a step increment of 1%. Each composition was prepared by weighing each compound using a Mettler Toledo scale with a weighing accuracy of ± 0.03 mg following the same protocol as detailed in sub-section 2.2 of [2]. The preparation of a sample involves melting the product to be analyzed and depositing small droplets of the product on the substrate. The substrate is a thin plate (thickness of 2mm, area of 11 cm x 7.5 cm) made either of aluminum or of brass. In the frame of the IRT method, the term sample refers to the ensemble {plate + droplets}. The use of droplets less than 20 mg is recommended in order to warrant that the temperature of the droplet is almost uniform and close to that of the substrate. Besides, a droplets spacing must be selected to avoid interference between them due to the heat released/absorbed by each droplet.

The experimental method is based on the observation *via* infrared thermography of the crystallized droplets melting submitted to a heating ramp. The IRT method for the determination of phase diagrams is thus a dynamic method correlating phase transitions to the emissivity changes occurring in a studied system [2].

When the observed material starts to crystallize/melt an abrupt change in the emissivity is expected, leading to a change in the trend of the DL-signals (see more details in [2]). When the phase change process is finished the emissivity becomes constant and the evolution of the signal with temperature is linear once again.

The obtained infrared movies are then analyzed (see in sub-section 2.4). The experimental setup is described in sub-section 2.3 of [2]. The main elements of this setup are:

- A programmable heating/cooling system on which the samples are placed, allowing covering temperatures ranging from -10°C to 200°C, coupled with a command system allowing for heating/cooling rates ranging from 1 to 10°C/min with a ± 0.1°C accuracy.
- A photonic IR camera FLIR X6580 sc (1.5 to 5 µm InSb cooled detector, 640 x 512 pixels resolution, 1-355Hz acquisition frequency).

2.2 Experiments

For the estimation of the phase diagram, the performed experiments presented in this work followed a protocol similar to the one proposed in [2]. The sample is placed on the heating plate mentioned in sub-section 2.1 and it is heated up following the thermal course sketched in Figure 1. The temperature at the surface of the plate is measured with a thermocouple, allowing to record, measure and control the temperature of the sample. This thermocouple is glued to the plate using silver paint and insulated from its environment using insulating foam. A first stage of 5min is performed at ambient temperature (T_{amb}) to ensure the sample equilibrium. Then, the sample is submitted to a heating ramp at a moderate rate (β = 1°C/min) in order to follow the assumption of equality between the temperature of the conductive plate and the temperature of the droplets. Finally, the sample is submitted to a last stage, around 15°C above the highest melting temperatures (T_m) of the 2 pure materials composing the binary system, to ensure that all droplets are liquid and that the sample is at equilibrium at the end of the experiment (after only 65 minutes).

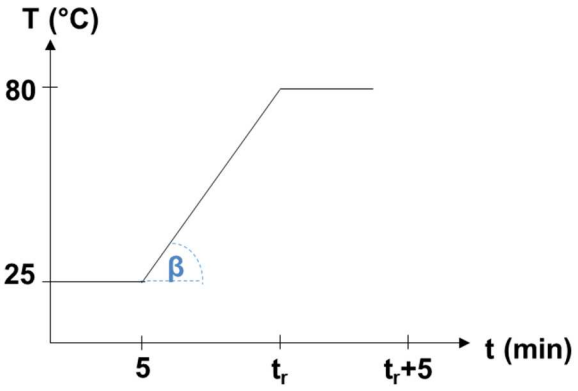

Fig. 1. Sketch of the thermal course applied to the sample during a heating experiment of 65 minutes duration (with t_r the end of the heating ramp).

The minimal temperature (ambient temperature: 25°C) and the maximal one (80°C) are selected so that all the crystallized CA-PA droplets melt within this interval of temperature. A low heating/cooling ramp of 1°C/min is applied on the same principle as for a DSC analysis. The plate being highly conductive, the heating rate being low, and the droplets being small (3 and 7mm), the temperature of the plate is assumed to be uniform and always equal to the temperature of the droplets. Therefore, the thermocouple placed on the plate is assumed to record the temperature of each droplet at any time and enables the association of a signal variation to a specific temperature.
During the heating ramp and up to its end (t_r), the IR camera records simultaneously and continuously the photonic flux emitted by each droplet on the plate. Its acquisition rate is set to 7 Hz to match the best compromise between the amount of gathered data and the processing time.

2.3 Tests carried out

Three series of experiments were performed.
The first one aims at estimating the experimental CA-PA phase diagram. The used substrate is a thin aluminum plate and the diameter of the deposited droplets was approximately of 7mm.

The second series aims at investigating the influence of the droplet size on the estimation of the CA-PA phase diagram. The samples consisted in droplets deposited on the same aluminum plate with two different sizes of droplets of 3 and 7mm (their sizes and weight are reported in Table 2 and a picture of them can be seen in Figure 2). The droplets spacing is of 9mm for the 3mm-droplets but was increased up to 2 cm for the 7mm-ones.

Fig. 2. Droplets of PA with diameters of 3 and 7mm at solid state (above) and liquid state (below).

Table 2

Droplet sizes, masses and spacings.

Droplet size (mm)	Droplet mass (mg)	Droplets Spacing (cm)
3.3 ± 0.01	1.76 ± 0.03	0.9 ± 0.01
7 ± 0.01	11.14 ± 0.03	2 ± 0.01

The last series aims at investigating the influence of the nature and the roughness of the substrate on the estimation of the CA-PA phase diagram. The roughness of the substrates' surface is measured with an HOMMELTESTER T500 roughnessmeter. The plate is placed on a heating element and roughness measurements are performed at temperatures ranging from 20°C to 65°C. To investigate the uniformity of the surfaces and to calculate uncertainties, the plates were divided in nine sections (Figure 3) and the measurements are carried out independently on each section. The roughness of a surface is evaluated through two statistical parameters: the average amplitude of the roughness (Rz) and the arithmetical mean of the distances (in absolute value) between the actual surface and the mean surface (Ra). No significant changes of roughness with temperature have been observed in the range of the tested temperatures. Obtained parameters Rz and Ra are reported in Table 3 [11].

The tested samples consist of 3mm-droplets deposited on two different plates made of aluminum and brass (see Figure 3). To perform this study on the influence of the nature and the surface condition of the conductive plate on the estimation of the same CA-PA phase diagram, we the results obtained with the same size of droplets (3mm diameters) deposited on two highly conductive plates with the same dimensions and with surfaces both polished with an 800 grit sandpaper. In addition, the plates are identical to the ones used in the frame of the SAM.SSA project and presenting a larger roughness difference between them while allowing for a uniform surface temperature [11].

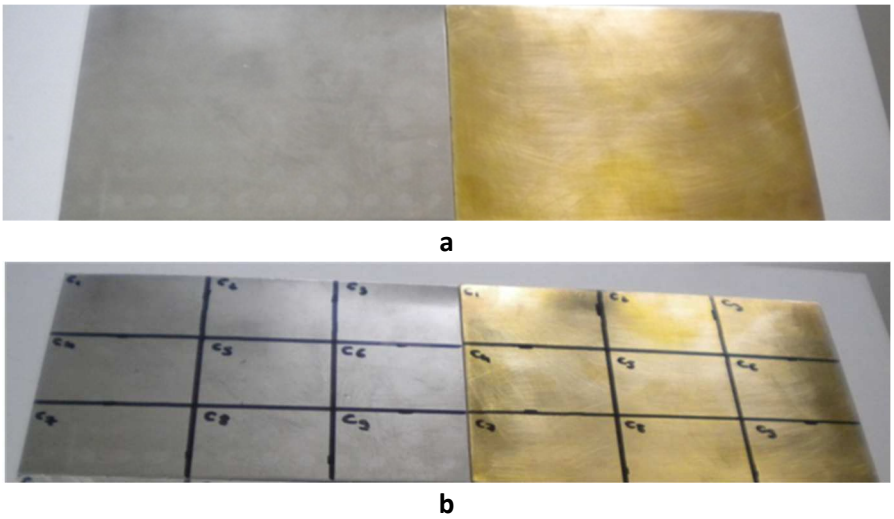

a

b

Fig. 3. Tested plates: a. Raw plates, made of aluminum on the left and of brass on the right ; b.tested plates divided in nine sections for the roughness measurements.

Table 3

Roughness measurements from 20°C to 65°C.

	Ra (µm)	**Rz (µm)**
Brass	0.135 ± 0.065	1.213 ± 0.527
Aluminum	0.667 ± 0.173	5.198 ± 0.978

2.4 Data treatment: Adaptation and automatization

The phase transitions are detected using the time-eigenfunctions for each droplet (see more details in [2]). A transition is associated to an abrupt change in the signal trend. This change can be detected using the Matlab function *findchangepts* described in [12]. It allows finding in a signal, the locations

where the deviation according to a chosen statistical parameter (mean, root-mean-square, standard deviation and linear) is maximal. Looking at the third eigenfunction of a droplet (see Figure 4a), one can rather easily identify transitions *via* the abrupt changes in the linearity of the signal. However, the noise in the raw signal makes the automation of the transition detection process unreliable and requires therefore a filtering step. Given the shape of the signal and after reviewing the Fourier transform of the signal it is concluded that an adequately designed lowpass filter can filter this higher frequency noise and provide the filtered eigenfunction as seen in Figure 4b.

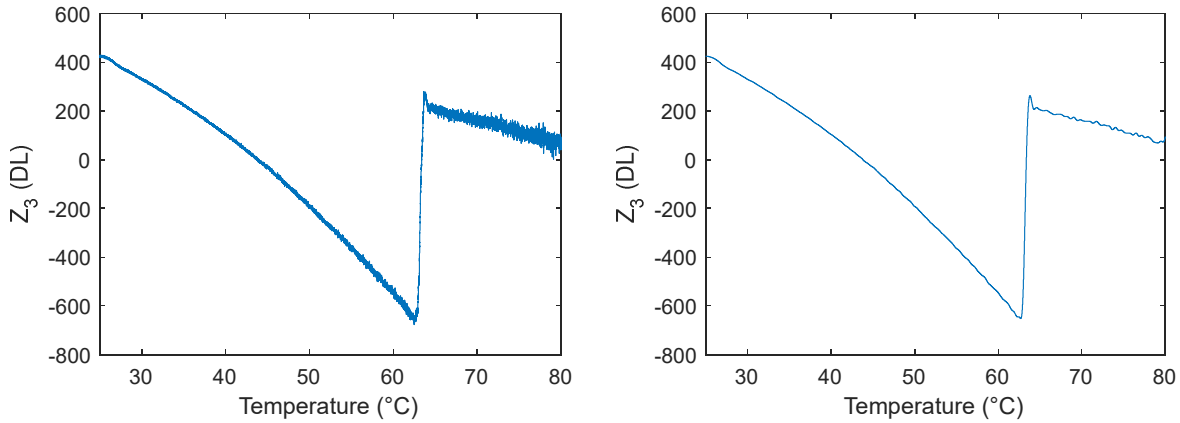

Fig. 4. Third eigenfunction for a CA-PA droplet with a 5%-95% molar composition a. Unfiltered. b. Filtered.

The Matlab function can now be used to find the location of the most abrupt changes in the linearity of the signal. Given that noise still remains in the right part of the filtered signal, this process is performed iteratively. First, the liquid-solid transition constituting the liquidus line is identified, then, transitions occurring at temperatures below this line are sought after (namely metatectic, peritectic or eutectic transitions). We see in Figure 5 that this method is successful in detecting a solid-liquid transition temperature at 63.1°C for this given sample. This temperature value is in the range of those that could have been picked manually. Besides, this transition temperature is also coherent with what is expected from a sample with this composition if we refer to DSC results presented in Section 3.

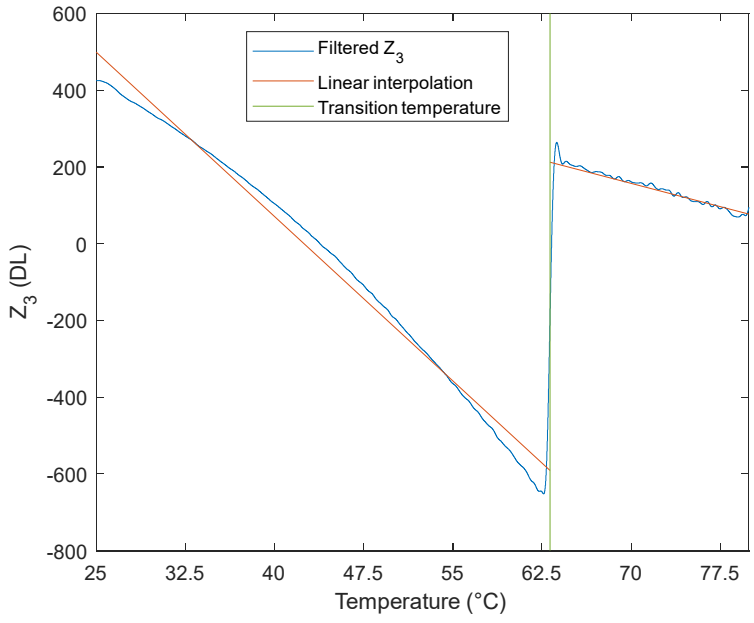

Fig. 5. Automated detection of the solid-liquid transition temperature on the third eigenfunction for a CA-PA droplet with a 5%-95% molar composition.

2.5 Validation

In addition to the comparison with data from literature, the obtained results using the improved IRT method are confronted to experimental ones collected from a DSC analysis performed with samples from the same batch as the droplets used during IRT experiments. Moreover, the results are also compared with an improved thermodynamic model to estimate the solid-liquid equilibrium of binary systems composed of organic materials and presenting a peritectic transition.

2.5.1 Thermodynamic modeling

The modeling of the solid-liquid equilibrium of fatty acids binary systems is complex for they do not only present metatectic and peritectic transitions but are also subject to polymorphism. The model used here, that was already described and applied for the Palmitic-Stearic acid system in [13], is given in Equation 1. It is a combination of the models found in [14] and [15], respectively presenting means of accounting for the polymorphic behavior of the compounds and considering the peritectic transition influence on the liquidus line shape.

$$\sum_i \ln(x_i \gamma_i^L) = \sum_i \nu_i \left(\frac{\Delta_m h_i}{R} \left(\frac{1}{T_m^i} - \frac{1}{T} \right) + \sum_{tr=1}^{n} \left(\frac{\Delta_{tr} h_i}{R} \left(\frac{1}{T_{tr}^i} - \frac{1}{T} \right) \right) \right) - \frac{\Delta_r G^0}{RT} \quad (1)$$

Where i is the pure component i, L characterize the liquid phase, x_i is the molar fraction of i in the liquid phase, γ_i is the activity coefficient of i in the liquid phase, R is the universal gas constant, T_m and $\Delta_m h$ are the temperature and enthalpy of melting respectively, T_{tr} and $\Delta_{tr} h$ are the temperatures and enthalpies of the different solid-solid transitions occurring for the component i respectively, ν_i are the stoichiometric coefficient associated to the reaction forming the peritectic compound and $\Delta_r G^0$ is Gibbs free energy of the peritectic reaction.

Equation 1 is valid to depict the solid-liquid equilibrium of a compound assimilated to the result of a stoichiometric reaction on the condition that the stoichiometry is known. This stoichiometry is unknown prior to the experiment but given the shape of the phase diagram given by the authors in [10] it can be approximately considered as a 1:1 stoichiometry. The Gibbs free energy of reaction is here a fitting parameter and the liquid activity coefficient, only unknown remaining besides the temperature, is calculated using the UNIFAC-Dortmund method described in [16].

We use the common model [17] described in Equation 2 to depict the part of the liquidus line not affected by the peritectic transition (using data from Table 1)**:**

$$\ln(x_i \gamma_i^L) = \frac{\Delta_m h_i}{R} \left(\frac{1}{T_m^i} - \frac{1}{T} \right) + \frac{\Delta_{tr} h_i}{R} \left(\frac{1}{T_{tr}^i} - \frac{1}{T} \right) \quad (2)$$

It implies that polymorphic transitions exist and that their temperatures and transition enthalpies are known. Most of the time and as indicated before, this is not the case and therefore the right-hand part of the model is limited to the first term. According to the authors in [18], Palmitic acid present a polymorphic behavior influenced by several factors such as crystallization rate and polarity in solution. Knowing which polymorphic transition to consider in this given case is difficult, as it requires an in-depth study of each compound and their interaction in a solution. Assuming a fast crystallization rate and considering that both components are weakly polar, [18] would indicate a

polymorphic transition T_{tr} = 51.5°C with a transition enthalpy around 2 600 J/mol. Those parameters considered in our model.

2.5.2 Differential Scanning Calorimetry (DSC)

For the DSC analysis, a DSC 131 supplied by Setaram is used at ambient atmosphere and the same 1°C/min ramp as for the IRT experiments is applied to validate the previously obtained data. A 10% increment is chosen for the compositions of validation points to limit the time spent on this procedure. It can indeed be very time-consuming if accurate results and/or several compositions are required. Moreover, two cycles are usually necessary to ensure the contact between the material and the crucible required for a homogeneous heating. The phase transitions are generally related to the heat flux evolution as a function of temperature. A peak appears when a specific process such as melting or crystallization occurs. The transition temperatures are extracted from the thermograms using the software SETSOFT2000. Regarding the determination of the transition temperatures on the thermograms, the guidelines recommended in [3,19] are followed. For pure or homogeneous samples where a clear transition peak, preceded and followed by a flat baseline, is identifiable, the onset temperature is considered as it is the best indicator of the beginning of the transition process. For mixtures/inhomogeneous samples, several transitions can take place successively or simultaneously. In such cases, clear peaks may not be obtained. It is therefore common to consider the peak temperature as an estimate of the transition temperature.

For some compositions (65% CA, 70% CA, 95% CA), we were not able to retrieve transition temperatures from the obtained thermograms. Therefore, we had to reduce the heating rate (β = 0.3°C/min for the 65% CA and 95% CA compositions and β = 0.1°C/min for the 70% CA composition) in order to obtain useable thermograms for the detection of transition temperatures.

3 Results

3.1 Phase diagram estimation

The experimental results obtained using infrared thermography are compared with literature ones [10] in Figure 6.

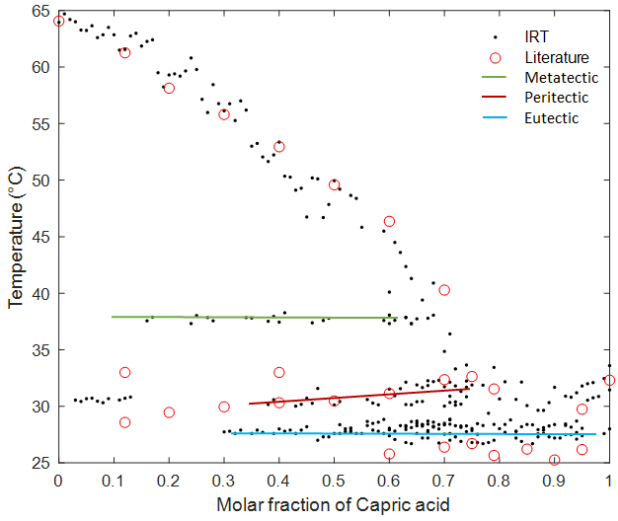

Fig. 6. Experimental phase diagram obtained with the IRT method and identification of the occurring transitions compared with literature data [10]

In Figure 7, experimental results obtained using infrared thermography are compared this time with results obtained *via* thermodynamic modeling (see sub-section 2.5.1 and [13]) and a standard technique (see sub-section 2.5.2).

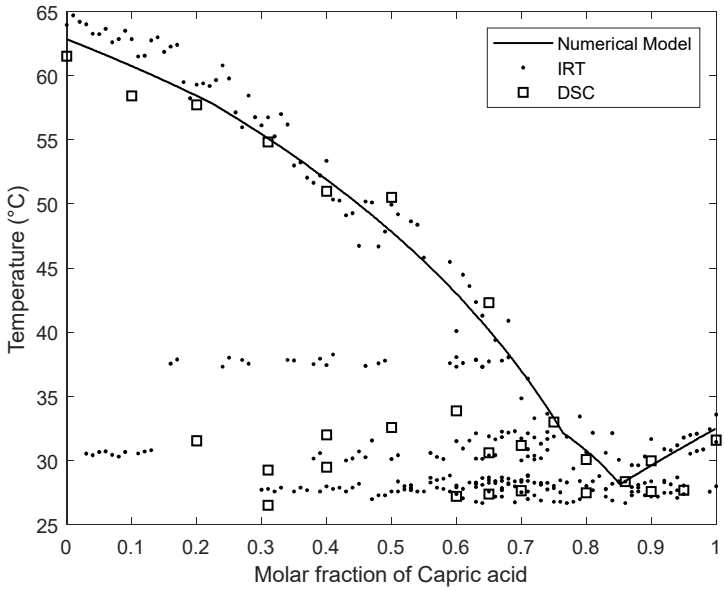

Fig. 7. Comparison between thermodynamical modeling, improved IRT and DSC experiments.

From Figures 6 and 7, we can notice that the improved IRT method was able to provide in a 1–hour experiment a phase diagram that is within acceptable range of literature data, DSC measurements and the proposed thermodynamic model. One could argue that the temperature difference between DSC results and IRT results from Figure 6 and 7 is rather large, especially on the left side of the diagram, near pure-component samples. As stated previously, for pure or homogeneous samples it is best suited to choose the onset temperature on the thermograms as the transition temperature. Authors in [10] preferred the peak temperature for all transition temperatures determination, hence the noticeable deviation. However, as we move away from pure-component samples to inhomogeneous samples, the temperature discrepancy becomes less noticeable as we now consider the peak temperature in the thermograms as well. The eutectic and peritectic transitions are in agreement with results obtained *via* the standard methods. As for the metatectic transition, it appears to be the most challenging transition to detect in this case (see sub-section 3.2) and its temperature has been overestimated by 2-3°C during our experiment when compared with literature data. It is however interesting to note that DSC measurements whether from literature or made in this work appear limited or incomplete as it is difficult from the thermograms to identify the peritectic or metatectic transitions. Their transition temperature being relatively close to each other, it possible that their peaks coincide or that one has a much higher enthalpy than the other and is consequently missed. Such issue could be an explanation as to why the metatectic transition was also poorly identified with the IRT method. Regarding the thermodynamic model, it was able to depict in a reliable way the liquidus line although it seems to drift away from it in the 0.5-0.7 molar fraction range.

3.2 Influence of the droplet size

The same CA-PA phase diagram is estimated for 2 droplet sizes, with 3mm and 7mm diameters, deposited on the same aluminum conductive plate in order to study the influence of the droplets size (see Figure 8).

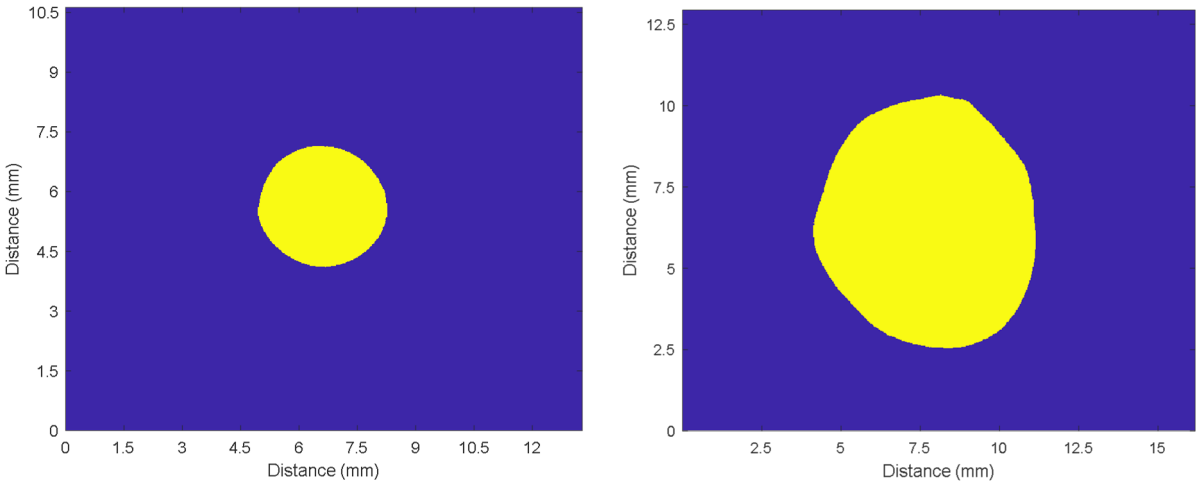

a **b**

Fig. 8. IR picture of a PA droplet with a diameter of a. 3mm, b. 7mm.

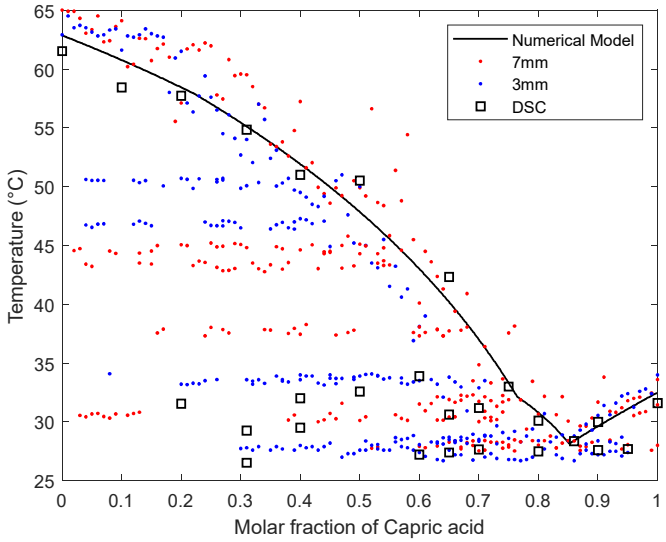

Fig. 9. Superposition of 2 estimations of the CA-PA phase diagram for droplets deposited on an aluminum plate with 2 droplets diameters: 7mm in red and 3mm in blue compared with DSC measurements and a thermodynamic model.

Although the estimated phase diagrams with two different sizes appear to have the same shape (see Figure 9), we notice significant differences in the estimated transition temperatures. The liquidus line is correctly depicted since IRT results and DSC measurements show the same pattern and adequately coincide. The detection of the peritectic and metatectic transitions is however subject to significant deviations. The IRT data obtained for both droplet sizes show discrepancies. On the one hand, both transitions are detected with the 7mm droplets. The peritectic transition is coherent with DSC measurements but the metatectic one has been overestimated by several degrees. On the other hand, a single transition is noticed with the 3mm droplets. Although its detection is consistent and

regular, it is difficult to say whether one transition is prioritized for the detection or if the detected transition is a combination of both peritectic and metatectic transitions. Additionally, the phase diagram obtained with larger droplets appears to depict a slightly more coherent liquidus line especially at lower temperatures. Hence, we study the influence of the droplet size on the recorded signals more precisely by observing the melting of a single droplet using the same IR camera, but this time equipped with a microscopic lens. As shown in Figure 10, the size of the droplet influences the time-eigenfunctions of the recorded signals.

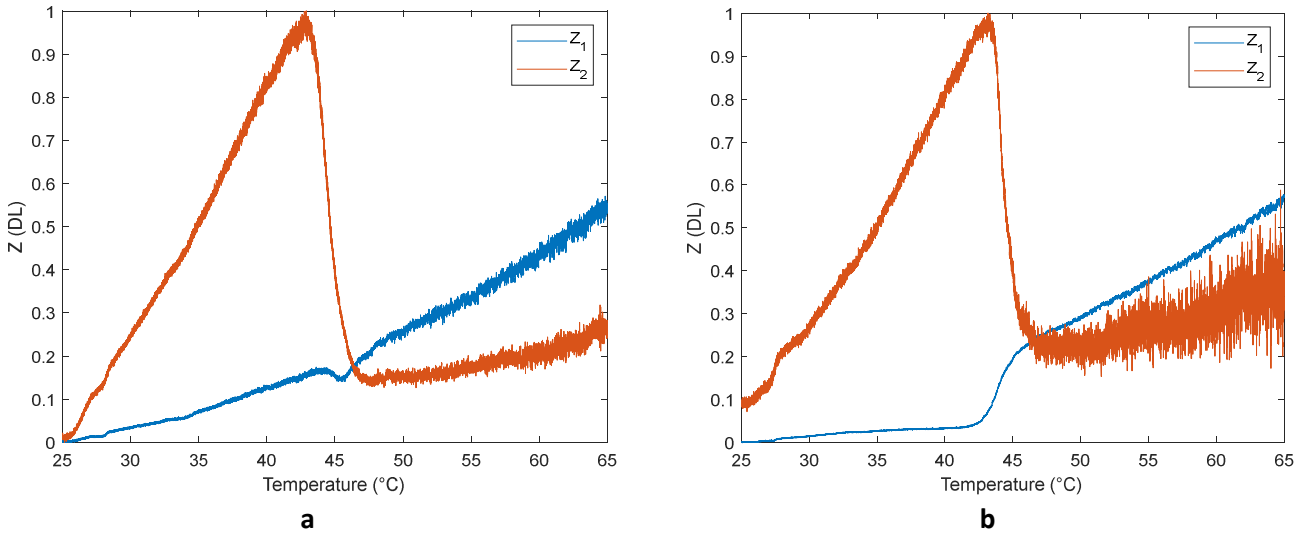

Fig. 10. Eigenfunctions Z obtained for the melting of 2 droplets of CA-PA with an equimolar composition with different diameters: a. 3mm and b. 7mm.

Figures 8a and 10a are the ones associated to the smallest droplet (with a diameter of 3 mm) and Figures 8b and 10b are the ones associated to the biggest one (with a diameter of 7mm). First, we notice that the variations related to phase transitions are more or less significant and spread. On the one hand, the DL-Temperature ratio is highly nonlinear, and on the other hand, variations can be drawn into the signal noise. When the variations are really spread, the signal treatment in itself is unlikely to give reliable information regarding the beginning of a transition and can therefore lead to temperatures varying from a few degrees.

While observing Figures 10a and 10b and especially with the first eigenfunction Z_1, we can notice that the variation indicating a phase transition is less spread in Figure 10a, representing the smallest droplet, than in Figure 10b. This is explained by the more uniform temperature repartition inside the smallest droplet, the ideal case being a homogeneous temperature. As explained in more details (sub-section 2.4), the data treatment is allowed by the extraction of the overall evolution of the temperature inside droplets. The phase transition and hence the induced heat exchange, does not occur at the same time at every location within the droplet. Consequently, we conclude that the larger the droplet, the higher the temperature difference inside the droplet is. A wettability study might as well be required since the weaker the wettability, the less flat the droplet is, which will involve higher observed temperature disparities (see the droplet shape in Figure 2).

From our previous observations, it appears that no matter the droplet size, the same transitions are detected on the exception of the metatectic one only observed for the droplet with a diameter of 7mm. However, the transition detection is steadier for the smaller droplets but the estimated temperatures present slight deviations with literature values or DSC measurements in comparison with larger droplets. The liquidus line seems to be depicted in a better way with larger droplets for which transitions below the peritectic transition temperature are easily noticed in the phase

diagram. An explanation of this phenomenon can be related to the transition kinetics. Because of their increased thermal inertia due to their size, the temperature is not reached uniformly within the droplet, but progressively. Therefore, a reaction occurring slowly is more likely to be noticed if a thermal gradient exists within the droplet. This could be the reason why a metatectic transition seems to have been noticed for the 7mm-droplet and not for the 3mm-one. Additionally, as the larger droplets provide more information, it is not surprising to notice the variation before the smaller droplets do. Although, at higher temperature the phenomenon tends to reverse as larger droplets are more affected by the ambient atmosphere due to their size. Consequently, a size compromise is to be found, large enough to obtain the optimal transition temperatures and liquidus shape but small enough to minimize the deviations between adjacent points and for a neat phase diagram. Another option could be to decrease the heating rate to let transitions take place or to limit the influence of the ambient conditions on the droplet temperature.

3.3 Influence of the nature of the plate

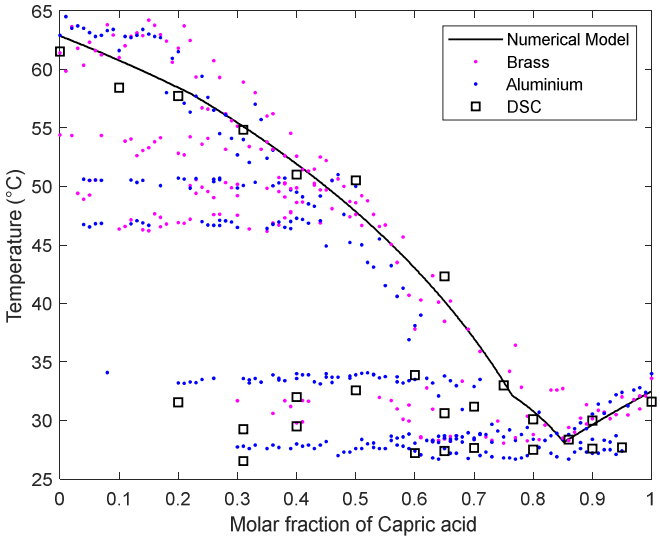

Fig. 11. Superposition of 2 estimations of the CA-PA phase diagram for droplets, with a diameter of 3mm, deposited on two different substrates: an aluminum plate in blue and a brass one in pink and comparison of the estimated phase diagrams with DSC measurement and a thermodynamic model.

Although the estimated phase diagrams with both conductive plates appear to be comparable (see Figure 11), there are significant differences in the estimated transition temperatures. It is therefore necessary to use the same plate to limit the impact of the surface condition.

The ideal situation would then be to optimize:

- The spacing between droplets to be able to deposit as much droplets as possible on the same plate.
- The size of the droplets to be more accurate in the transition temperatures estimation.
- To always use the same conductive plate to ensure the same surface condition.

4 Discussion

The thermodynamic model successfully shows the influence of the peritectic transition on the shape of the liquidus line and appears to be rather accurate especially for compositions rich in one or the other component. However, an increasing deviation can be noticed as the liquidus approaches the metatectic transitions. This could be explained by the fact that the model assumes complete

immiscibility in the solid phase which is in contradiction with the presence of a metatectic transition. In addition, from the phase diagram given in the literature [10], it appears that the solid solubility domain is not negligible. Consequently, this assumption is to be revisited as the influence of a metatectic transition or solid solubility appears to be not negligible. Additionally, the polymorphic data for fatty acids and organic compounds in general is still lacking. Although, the polymorphic transition influence did not have a major impact on the depiction of the liquidus line in this case, it can lead to consequent deviations in some cases. It should be noted that transitions appear to be detected between the liquidus line and the metatectic transition, as can be seen in Figures 9 and 11. As explained previously, the Palmitic acid is a polymorphic material and according to [18], multiple polymorphs exist amongst which some have coincident transition temperatures with those detected by the IRT method. In this study it is chosen to disregard those transitions as they were not backed by any DSC measurements but this aspect might be worth investigating in further works.

The data treatment automation when it comes to determining transition temperatures has proven to be effective when looking for the melting temperature. For lower transitions temperatures, the results are highly dependent on the transition energy. Indeed, transitions with a lower energy are difficult to detect as they can be drawn into the remaining filtered noise. Additionally, the obtained results can be different depending on which time-eigenfunction is studied and therefore a different treatment may be needed for each eigenfunction.

As mentioned previously, our study on the influence of the droplet size, substrate material and surface condition shows that a compromise regarding droplet size is to be found to optimize the IRT method and to provide phase diagrams of increasing accuracy. As observed for the DSC measurements, reducing the heating rate is needed in order to be able to detect the transitions. Therefore we can imagine reducing the rate from 1°C/min to 0.5°C/min which brings the IRT experiment duration to around 2 hours which is still extremely competitive in comparison with traditional methods. Another option could be to have a preliminary run with smaller droplets to have a preliminary phase diagram, completed then by another run with larger droplets for selected composition ranges. This would provide an estimated phase diagram in a 2-3 hours experiment when it could take weeks with standard methods.

5 Conclusion

The application of the IRT method for the preliminary estimation of more complex phase diagrams has proven to be successful, identifying solid-liquid, eutectic, peritectic and even metatectic transitions in only a one hour experiment.

Our study led us to assess the influence of different parameters on the efficiency of the method to identify optimal parameters as well as limiting factors. We showed that the droplet size has a significant impact on the phase diagram estimation. A preliminary study must be performed to identify the optimized droplet size for each studied binary system. This fast experiment consists in observing the melting of a droplet and in studying the thermal behavior of each pixel within the droplet in order to make sure that the droplet is large enough so that the transitions influence the emitted photonic flux but not too large to ensure temperature homogeneity inside the droplet. We also noticed that the surface condition of the plate can influence the estimation, it is therefore important to use the same plate if we are to set consistent protocols up and obtain reproducible results.

The automated treatment of the recorded signals has shown good results, accurately determining most transitions. There is still room for improvement however as detecting lower energy transition is

still challenging. In addition, the time-eigenfunctions behave and evolve differently and therefore a different treatment for each eigenfunction can be considered for better results.

An improved thermodynamic model was used to replicate the liquidus line for this binary system. Although, this approach provided rather accurate results, significant deviations were measured when the solid solubility increased. Consequently, the assumptions of this model are to be revisited. Additionally, the data regarding polymorphic behavior of organic compounds is lacking and can be problematic for compounds with high polymorphic transition enthalpies.

Acknowledgments

This work is carried out in the frame of SUDOKET project and is co-funded by the Interreg Sudoe Programme through the European Regional Development Fund (ERDF).

References

[1] J. Zhao, M.R. Notis, Phase transformation kinetics and the assessment of equilibrium and metastable states, J. Phase Equilib. 14 (1993), 303-315.
[2] E. Palomo del Barrio, R. Cadoret, J. Daranlot, F. Achchaq, Infrared thermography method for fast estimation of phase diagrams, Thermochimica Acta, 625 (2016), 9-19.
[3] L. Rycers, Practical remarks concerning phase diagrams determination on the basis of differential scanning calorimetry measurements, J. Therm. Anal. Calorim. 113 (2013), 231-238.
[4] E. Gunther, S. Hiebler, H. Melhing, R. Redlich, Enthalpy of phase change materials as a function of temperature: Required accuracy and suitable measurement methods, Int. J. Thermophys. 30 (2009), 1257-1269.
[5] T. Kousksou, A. Jamil, Y. Zeraouli, J-P. Dumas, Equilibrium liquidus temperatures of binary mixtures from differential scanning calorimetry, Chem. Eng. Sci. 62 (2007), 6516-6523.
[6] E. Palomo del Barrio, R. Cadoret, J. Daranlot, F. Achchaq, New sugar alcohols mixtures for long-term thermal energy storage applications at temperatures between 70°C and 100°C, Solar Energy Materials and Solar Cells 155 (2016), 454-468.
[7] Sigma Aldrich, website: https://www.sigmaaldrich.com/france.html, date of last connection: 28/08/2017
[8] K. Pielichowska, and K. Pielichowski, Phase change materials for thermal energy storage, Progress in Materials Science 65 (2014), 67-123.
[9] M. M. Kenisarin, Thermophysical properties of some organic phase change materials for latent heat storage. A review, Solar Energy 107 (2014), 553-75.
[10] M.C. Costa, M.P. Rolemberg, A.J.A. Meirelles, J.A.P. Coutinho, M.A. Krähenbühl, The Solid–liquid Phase Diagrams of Binary Mixtures of Even Saturated Fatty Acids Differing by Six Carbon Atoms, Thermochimica Acta 496 (2009) 30-37.
[11] M. Duquesne, A. Godin, E. Palomo del Barrio, J. Daranlot, Experimental analysis of heterogeneous nucleation in undercooled melts by infrared thermography, Quantitative InfraRed Thermography Journal 12 (2015), 112-126.
[12] Mathworks®, (2018). Signal Processing Toolbox™: Reference (R2018a), Retrieved August 31, 2018 from https://fr.mathworks.com/help/pdf_doc/signal/signal_ref.pdf
[13] C. Mailhé, I. Mahroug, M. Duquesne, A. Godin, E. Palomo del Barrio, F. Achchaq, M. Azaiez, Phase diagrams of fatty acids as biosourced phase change materials for thermal energy storage, Proceedings of the International Conference On Materials And Energy ICOME 2018, France, May 2018.

[14] D. Fernanda Barbosa and P. de Alcântara Pessôa Filho. On the Description of the Liquidus Line of Systems Presenting Peritectic Reactions, Fluid Phase Equilibria 337 (2013), 379-383.
[15] G. J. Maximo, R. T. Aquino, A. J. A. Meirelles, M. A. Krähenbühl, and M. C. Costa, Enhancing the description of SSLE data for binary and ternary fatty mixtures, Fluid Phase Equilibria 426 (2016), 119-130.
[16] J. Gmehling, J. Li, and M. Schiller, A modified UNIFAC model. 2. Present parameter matrix and results for different thermodynamic properties, Ind. Eng. Chem. Res. 32 (1993), 178-193.
[17] G. J. Maximo, M. C. Costa, and A. J. A. Meirelles, The Crystal-T algorithm: a new approach to calculate the SLE of lipidic mixtures presenting solid solutions, Phys. Chem. Chem. Phys. 16 (2014), 16740-16754.
[18] E. Moreno, R. Cordobilla, T. Calvet, M. A. Cuevas-Diarte, G. Gbabode, P. Negrier, D. Mondieig, and H. A. J. Oonk, Polymorphism of even saturated carboxylic acids from n-decanoic to n-eicosanoic acid, New Journal of Chemistry 31 (2007), 947-957.
[19] W. J. Boettinger, U. R. Kattner, K.-W. Moon, and J. Perepezko, NIST Recommended Practice Guide: DTA and Heat-Flux DSC Measurements of Alloy Melting and Freezing | NIST, Methods for Phase Diagram Determination, 2006.